NEURAL BLOCH EIGENSOLVER FOR HONEYCOMB LATTICES

Haaris Mian
Columbia University
ham2176@columbia.edu

ABSTRACT

This work presents a physics-informed approach to solving the Schrödinger eigenvalue problem associated with particles in two-dimensional periodic potentials, with a focus on honeycomb lattice geometry, due to its non-trivial band topology and relevance to materials such as graphene. By leveraging neural networks to learn complex Bloch functions and their associated eigenvalues (energies) simultaneously, we develop a mesh-free neural solver enforcing the governing PDE, Bloch periodicity, and normalization constraints through a composite loss function without supervision. The model is numerically benchmarked against traditional plane-wave expansion methods. We also explored transfer learning to adapt the solver from nearly-free electron potentials to strongly varying potentials, demonstrating its ability to capture changes in band structure topology. This work contributes to the growing field of physics-informed machine learning for quantum eigenproblems, providing insights into the interplay between symmetry, band structure, and neural architecture.

1 INTRODUCTION

Recently, there has been growing interest in leveraging the techniques of scientific machine learning to solve partial differential equations (PDEs) that arise in physics and engineering. One approach that has shown promise is the use of physics-informed neural networks (PINNs), which allow for the incorporation of governing equations and physical constraints directly into the loss function of a neural network (Raissi et al., 2017). This framework has been successfully applied to a variety of problems, including fluid dynamics, materials science, and quantum mechanics (Karniadakis et al., 2021; Cai et al., 2021; Jin et al., 2020).

In this paper, we develop a physics-informed approach to the time-independent Schrödinger equation for particles in a 2D periodic potential, an eigenvalue problem of fundamental importance in condensed matter physics and materials science. The theory of electrons in periodic potentials, described by Floquet-Bloch theory, underpins our understanding of the electronic properties of crystalline solids (Ashcroft & Mermin, 2011). Notably, certain lattice structures, such as the honeycomb lattice found in graphene, exhibit conical degeneracies in their band structure known as Dirac points (Fefferman & Weinstein, 2012; Lee-Thorp et al., 2018). These points give rise to unique transport properties which have been the subject of extensive theoretical and experimental investigation.

Traditional numerical methods, such as finite element methods, can be computationally expensive for high-dimensional settings and rely on a mesh discretization of the domain. In this work, we aim to create mesh-free solvers that can recover both eigenvalues and eigenfunctions of the Schrödinger equation in honeycomb symmetric potentials.

The main contributions include: (1) Physics-informed learning framework for solving the Floquet-Bloch eigenvalue problem in two-dimensional periodic potentials, with a focus on honeycomb lattice geometry; (2) Objective enforcing PDE residuals, boundary conditions, and normalization constraints for physically valid eigenstates, as well as Bloch inductive bias; (3) Numerical validation of neural network solutions with traditional numerical (spectral) methods, demonstrating their ability to accurately capture band structure topology.[1]

[1] Code is available at github.com/haarisamian/neural-bloch-eigensolver

2 METHODS

2.1 NEURAL PARAMETERIZATION OF BLOCH EIGENFUNCTIONS

We begin by defining a neural network to approximate the Bloch functions $u_{n,\mathbf{k}}(\mathbf{x})$ over the unit cell Ω for a given quasi-momentum $\mathbf{k}$ in the Brillouin zone (Additional detail on Floquet theory in Appendix B). The model takes as input the spatial coordinates $\mathbf{x} \in \Omega$ and the quasi-momentum $\mathbf{k}$ in reciprocal space, and outputs the complex-valued Bloch function $u_{n,\mathbf{k}}(\mathbf{x})$. To handle the complex amplitude, we represent the output as two real-valued components corresponding to the real and imaginary parts:

$$\mathcal{N}_1(\mathbf{x}, \mathbf{k}; \theta) = \begin{pmatrix} u^{\text{Re}}_{n,\mathbf{k}}(\mathbf{x}) \\ u^{\text{Im}}_{n,\mathbf{k}}(\mathbf{x}) \end{pmatrix}, \tag{1}$$

as well as an associated eigenvalue network:

$$\mathcal{N}_2(\mathbf{k}; \phi) = E_{n,\mathbf{k}}, \tag{2}$$

where θ and ϕ denote the trainable parameters of the respective networks. The full Bloch wavefunction can then be reconstructed using equation 13:

$$\psi_{n,\mathbf{k}}(\mathbf{x}) = e^{i\mathbf{k}\cdot\mathbf{x}} \left[u^{\text{Re}}_{n,\mathbf{k}}(\mathbf{x}) + i u^{\text{Im}}_{n,\mathbf{k}}(\mathbf{x}) \right]. \tag{3}$$

We note a subtlety here relating to the multiple bands, which can been handled in two ways: either by training separate networks iteratively with orthogonality constraints in the spirit of Jin et al. (2022), or by employing a single network, where the higher energy bands and Bloch modes can be discovered simultaneously through extended sampling of the Brillouin zone, as in Hsu & Mattheakis (2024). In this work, we focus on the latter approach, as it allows for more efficient training and exploration of the band structure topology with minimal architectural complexity. See Appendix A for extended related work on PINNs for eigenvalue problems.

2.2 LOSS FORMULATION

The training objective is formulated as a weighted sum of multiple loss components that enforce the physical constraints of the Floquet-Bloch eigenvalue problem. Specifically, we define the total loss $\mathcal{L}$ as:

$$\mathcal{L} = \mathcal{L}_{\text{PDE}} + \lambda_{\text{norm}} \mathcal{L}_{\text{norm}} + \lambda_{\text{BC}} \mathcal{L}_{\text{BC}}, \tag{4}$$

where $\mathcal{L}_{\text{PDE}}$ penalizes the residual of the Schrödinger equation, $\mathcal{L}_{\text{norm}}$ enforces normalization of the Bloch functions, and $\mathcal{L}_{\text{BC}}$ imposes the Bloch periodicity conditions. Proper balancing of these terms helps ensure convergence to physically valid solutions in a notoriously ill-conditioned optimization landscape (Krishnapriyan et al., 2021).

There is no universal recipe for the choice of weights which guarantees convergence to good minima in all settings, and ultimately they must be set empirically for each problem or chosen according to some adaptive self-weighting scheme. Here, they have been set empirically as $\lambda_{\text{norm}} = 100$ and $\lambda_{\text{BC}} = 10$ based on preliminary experiments to balance the contributions of each term during training.

2.2.1 SCHRÖDINGER PDE RESIDUAL

At each iteration of training, we sample a batch of collocation points $\{\mathbf{x}_i\}_{i=1}^{N_b}$ uniformly at random from the unit cell Ω and a batch of quasi-momenta $\{\mathbf{k}_j\}_{j=1}^{N_b}$ uniformly from the Irreducible Brillouin Zone (IBZ) and its lattice translates. Passing these through the networks, we compute the mean squared residual of the modified Schrödinger equation in equation 15:

$$\mathcal{L}_{\text{PDE}} = \frac{1}{N_b} \sum_{i=1}^{N_b} \left| \mathcal{H}_b \mathcal{N}_1(\mathbf{x}_i, \mathbf{k}_i; \theta) - \mathcal{N}_2(\mathbf{k}_i; \phi) \mathcal{N}_1(\mathbf{x}_i, \mathbf{k}_i; \theta) \right|^2, \tag{5}$$

where the Hamiltonian operator $\mathcal{H}_b$ is applied using automatic differentiation supported by `PyTorch` with respect to the spatial inputs $\mathbf{x}$.

2.2.2 Normalization Constraints

To ensure that the learned Bloch functions are physically valid eigenstates, and to avoid the trivial zero solution, we enforce the following normalization condition over the unit cell Ω:

$$\mathcal{L}_{\text{norm}} = \frac{1}{N_n} \sum_{i=1}^{N_n} \left(\int_{\Omega} |\mathcal{N}_1(\mathbf{x}, \mathbf{k}_i; \theta)|^2 \, d\mathbf{x} - 1 \right)^2, \tag{6}$$

where $\{\mathbf{k}_i\}_{i=1}^{N_n}$ are sampled quasi-momenta from the Brillouin zone, and the integral is numerically approximated using a trapezoidal rule over a fixed grid of points in Ω. We also note the added benefit that the squared amplitude of resulting eigenfunctions can be interpreted as a probability density.

2.2.3 Bloch Periodicity Conditions

Due to Bloch's theorem, the wavefunctions must satisfy the pseudo-periodic boundary conditions in equation 14. Or equivalently, the Bloch functions must be periodic over the unit cell. To enforce this, we sample points on the boundaries of the unit cell and compute the mean squared error between the values of the Bloch function at opposite boundaries:

$$\mathcal{L}_{\text{BC}} = \frac{1}{N_b} \sum_{i=1}^{N_b} |\mathcal{N}_1(\mathbf{x}_i + \mathbf{a_j}, \mathbf{k}_i; \theta) - \mathcal{N}_1(\mathbf{x}_i, \mathbf{k}_i; \theta)|^2 . \tag{7}$$

2.3 Model Architecture

While many architectural choices are possible, we opt for fully-connected feedforward neural networks due to their universal approximation capabilities and ease of implementation. The Bloch function network $\mathcal{N}_1$ takes the spatial coordinates $\mathbf{x}$ and quasi-momentum $\mathbf{k}$, and outputs the real and imaginary components of the Bloch function. The eigenvalue network $\mathcal{N}_2$ is similarly structured but takes only the quasi-momentum $\mathbf{k}$ as input and outputs the corresponding eigenvalue $E_{n,\mathbf{k}}$. Dimensions of the hidden layer is set to 200 with 5 hidden layers for the Bloch net, and 64 with 3 hidden layers for the energy net, and SiLU is chosen for an activation function.

3 Results

3.1 Band Structure Recovery for Honeycomb Potential

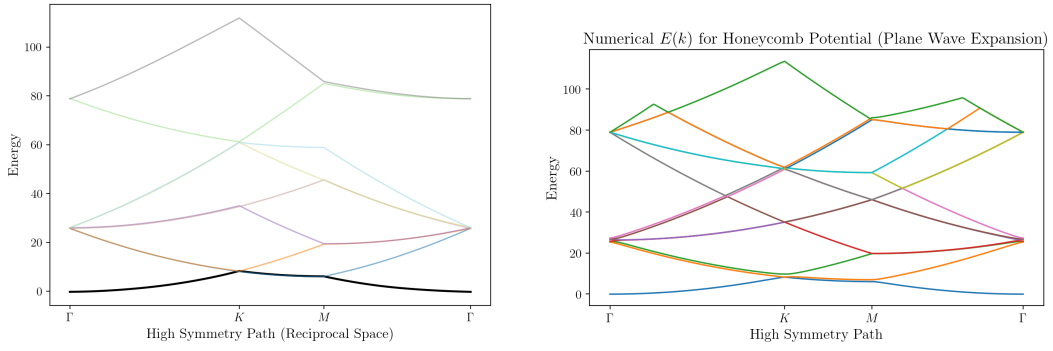

Figure 1: Band structure learned by the physics-informed neural network plotted along the high-symmetry path $\Gamma \to K \to M \to \Gamma$ in the Brillouin zone for a weak honeycomb potential with $V_0 = 1$. The learned dispersion curves (left) match closely with those obtained from the plane-wave expansion method (right), and closely approximate the free particle dispersion due to the weak potential.

After training the networks on a weak honeycomb lattice potential of the form $V(\mathbf{x}) = V_0 \sum_{i=1}^{3} \cos(\mathbf{b_i} \cdot \mathbf{x})$ with $V_0 = 1$, we evaluate the band structure using the trained eigenvalue

network $\mathcal{N}_2(\mathbf{k};\phi)$ over a dense sampling of $\mathbf{k}$-points along the high-symmetry path and its lattice shifted copies. The resulting dispersion curves are then compared to those obtained from the plane-wave expansion method to assess the accuracy of the neural solver in capturing the band structure topology. The learned band structure exhibits excellent agreement with the benchmark results from the plane-wave expansion method. The dispersion curves closely follow the expected behavior for a nearly-free electron model, with minor deviations attributable to the weak potential perturbation.

3.2 Error Metrics and Convergence Analysis

Loss metrics are tracked during training to assess convergence behavior both for the overall loss and individual components, which is crucial for diagnosing potential issues in optimization. The final values for the PDE residual, normalization error, and boundary condition error are reported in Table 1, demonstrating the model's ability to satisfy the governing physics of the problem.

Loss Component	Final Value
Total Loss ($\mathcal{L}$)	5.2×10^{-3}
PDE Residual ($\mathcal{L}_{\text{PDE}}$)	3.3×10^{-3}
Normalization Error ($\mathcal{L}_{\text{norm}}$)	3.0×10^{-7}
Boundary Condition Error ($\mathcal{L}_{\text{BC}}$)	1.9×10^{-4}

Table 1: Final loss values after training on weak ($V_0 = 1$) honeycomb potential.

3.3 Visualization of Bloch Functions

We also visualize the spatial profiles of the Bloch modes at select high-symmetry points Γ, K, and M. The squared amplitude is plotted over the unit cell to illustrate the probability density distribution of the electrons in these states. We include one representative state produced by the model which shows good qualitative agreement with numerical solutions.

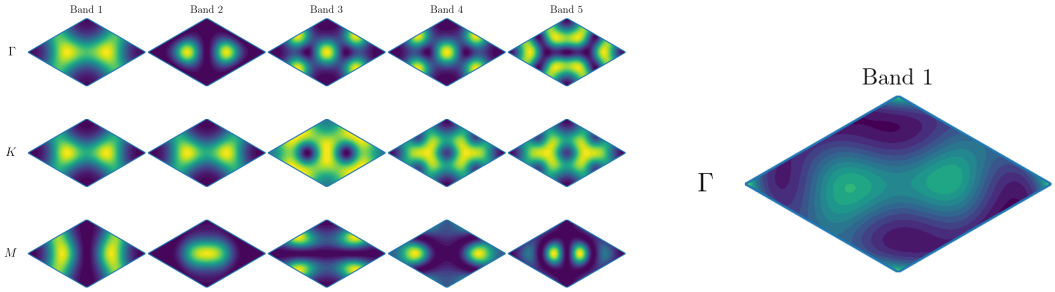

Figure 2: Representative Bloch modes plotted as $|u_{n,\mathbf{k}}(\mathbf{x})|^2$ over the unit cell at the high-symmetry points computed using the plane-wave expansion, as well as a representative Bloch state learned by the model at the Γ point after fine-tuning on $V_0 = 10$ (right).

4 Conclusion

We have developed a physics-informed neural framework for solving the Floquet-Bloch eigenvalue problem for honeycomb lattice potentials, demonstrating its ability to accurately recover band structures and Bloch functions for weak potentials. The model's predictions closely match benchmark results from the plane-wave expansion method, validating the effectiveness of the approach.

Future work may explore extensions to stronger potentials including pseudo-atomic well-like potentials and higher-dimensions. Fourier feature embeddings, as in (Sallam & Fürth, 2023), and other architectural enhancements may also be investigated to improve convergence and accuracy. Potentially, L-BFGS could be tried after convergence with Adam to improve the precision on the approach here. Overall, this work highlights the potential of physics-informed neural networks as a powerful tool for studying quantum materials with complex periodic potentials.

REFERENCES

Neil W. Ashcroft and N. David Mermin. *Solid State Physics*. Cengage Learning, 2011.

Shengze Cai, Zhiping Mao, Zhicheng Wang, Minglang Yin, and George Em Karniadakis. Physics-informed neural networks (pinns) for fluid mechanics: A review. *Acta Mechanica Sinica*, 37(12): 1727–1738, 2021.

A. H. Castro Neto, F. Guinea, N. M. R. Peres, K. S. Novoselov, and A. K. Geim. The electronic properties of graphene. *Reviews of Modern Physics*, 81(1):109–162, January 2009. ISSN 1539-0756. doi: 10.1103/revmodphys.81.109. URL http://dx.doi.org/10.1103/RevModPhys.81.109.

Salah A Faroughi, Nikhil M Pawar, Celio Fernandes, Maziar Raissi, Subasish Das, Nima K Kalantari, and Seyed Kourosh Mahjour. Physics-guided, physics-informed, and physics-encoded neural networks and operators in scientific computing: Fluid and solid mechanics. *Journal of Computing and Information Science in Engineering*, 24(4):040802, 2024.

Charles Fefferman and Michael Weinstein. Honeycomb lattice potentials and Dirac points. *Journal of the American Mathematical Society*, 25(4):1169–1220, October 2012. ISSN 0894-0347, 1088-6834. doi: 10.1090/S0894-0347-2012-00745-0. URL https://www.ams.org/jams/2012-25-04/S0894-0347-2012-00745-0/.

Jiequn Han, Arnulf Jentzen, and Weinan E. Solving high-dimensional partial differential equations using deep learning. *Proceedings of the National Academy of Sciences*, 115(34):8505–8510, 2018.

Circe Hsu and Marios Mattheakis. Equation-driven Neural Networks for Periodic Quantum Systems. 2024.

Henry Jin, Marios Mattheakis, and Pavlos Protopapas. Unsupervised neural networks for quantum eigenvalue problems. *arXiv preprint arXiv:2010.05075*, 2020.

Henry Jin, Marios Mattheakis, and Pavlos Protopapas. Physics-Informed Neural Networks for Quantum Eigenvalue Problems, February 2022. URL http://arxiv.org/abs/2203.00451. arXiv:2203.00451 [cs].

George Em Karniadakis, Ioannis G Kevrekidis, Lu Lu, Paris Perdikaris, Sifan Wang, and Liu Yang. Physics-informed machine learning. *Nature Reviews Physics*, 3(6):422–440, 2021.

Diederik P. Kingma and Jimmy Ba. Adam: A method for stochastic optimization, 2017. URL https://arxiv.org/abs/1412.6980.

Charles Kittel. *Introduction to Solid State Physics*. Wiley, 2004.

Aditi Krishnapriyan, Amir Gholami, Shandian Zhe, Robert Kirby, and Michael W Mahoney. Characterizing possible failure modes in physics-informed neural networks. *Advances in neural information processing systems*, 34:26548–26560, 2021.

J. P. Lee-Thorp, M. I. Weinstein, and Y. Zhu. Elliptic operators with honeycomb symmetry: Dirac points, edge states and applications to photonic graphene. *Archive for Rational Mechanics and Analysis*, 232(1):1–63, October 2018. ISSN 1432-0673. doi: 10.1007/s00205-018-1315-4. URL http://dx.doi.org/10.1007/s00205-018-1315-4.

Allan Pinkus. Approximation theory of the MLP model in neural networks. *Acta Numerica*, 8: 143–195, January 1999. ISSN 1474-0508, 0962-4929. doi: 10.1017/S0962492900002919. URL https://www.cambridge.org/core/journals/acta-numerica/article/abs/approximation-theory-of-the-mlp-model-in-neural-networks/18072C558C8410C4F92A82BCC8FC8CF9.

Maziar Raissi, Paris Perdikaris, and George Em Karniadakis. Physics Informed Deep Learning (Part I): Data-driven Solutions of Nonlinear Partial Differential Equations, November 2017. URL http://arxiv.org/abs/1711.10561. arXiv:1711.10561 [cs].

M. Reed and B. Simon. *Methods of Modern Mathematical Physics. IV Analysis of Operators*. Academic Press, New York, 1978.

Omar Sallam and Mirjam Fürth. On the use of fourier features-physics informed neural networks (ff-pinn) for forward and inverse fluid mechanics problems. *Proceedings of the Institution of Mechanical Engineers, Part M: Journal of Engineering for the Maritime Environment*, 237(4): 846–866, 2023.

A Extended Related Work: PINNs for Eigenvalue Problems

Physics-informed neural networks (PINNs), first introduced by Raissi et al. (Raissi et al., 2017), leverage the universal approximation capabilities of neural networks (Pinkus, 1999) to solve forward and inverse PDE problems through direct incorporation of governing physical relations into the optimization objective. This is typically implemented by defining a neural network that approximates the solution to the PDE and then formulating a multi-term weighted objective, known as the loss function, which penalizes deviations in the form of PDE residuals, boundary conditions, initial conditions (if applicable), and data mismatch (if available) as *soft constraints* on the network's output.

By training the network to minimize this loss through iterated sampling of the input space and reweighting of the parameters, typically with a stochastic optimizer such as Adam, the model learns to satisfy the underlying physics of the problem. These methods have the key advantage of being mesh-free, unlike traditional numerical methods such as finite element or finite difference methods, as well as the promise of greater efficiency in high-dimensional settings, which suffer from the so-called *curse of dimensionality* (Han et al., 2018; Raissi et al., 2017).

This approach has since been extended and applied to a variety of domains with notable success, including fluid dynamics (Cai et al., 2021), material science (Faroughi et al., 2024), and more recently, quantum mechanics (Jin et al., 2020; 2022; Hsu & Mattheakis, 2024). In recent years, there has been increasing attention to physics-informed learning for eigenvalue problems, such as are frequently encountered in physics and engineering, exemplified here by the time-independent Schrödinger equation. In this setting, the goal is to learn eigenvalues and eigenfunctions of differential operators or to find eigenfunctions for a predetermined eigenvalue. Notably, Jin et al. developed a PINN framework for solving quantum eigenvalue problems with square-well and Coulomb potentials, as well as a scanning neural network approach to learn multiple energetic eigenstates of the infinite square well and quantum harmonic oscillator (Jin et al., 2020; 2022).

However, to the best of our knowledge, there has been only limited exploration of physics-informed neural solvers for more general two-dimensional periodic quantum eigenproblems, as most works have tended to focus on one-dimensional wells or quantum harmonic oscillators. The setting of honeycomb lattice potentials and their spectral properties provide a rich testbed for studying the interplay between symmetry and band structure degeneracy in quantum materials. The closest such work is Hsu & Mattheakis (2024), who studied equation-driven (i.e. unsupervised) neural solvers for the Bloch eigenvalue problem for square lattices using constant and pseudo-atomic potentials. In a similar spirit, this work aims to extend this line of research by developing a physics-informed neural framework specifically tailored to honeycomb lattice potentials and their associated dispersion features, with an exploration of the benefits of transfer learning with pretraining on nearly-free electron potentials to generalize to strongly varying potentials.

B A Review of Floquet-Bloch Theory

We introduce some relevant results from the theory of periodic quantum media here as background (Reed & Simon, 1978). If we choose a linearly independent basis $\{\mathbf{a_1}, \mathbf{a_2}\}$ of $\mathbb{R}^2$ in real space, we can consider the lattice spanned by these vectors:

$$\Lambda = \{c_1\mathbf{a_1} + c_2\mathbf{a_2} : c_1, c_2 \in \mathbb{Z}\}, \tag{8}$$

as well as the reciprocal space (or *dual*) lattice:

$$\Lambda^* = \{c_1\mathbf{k_1} + c_2\mathbf{k_2} : c_1, c_2 \in \mathbb{Z}\}, \tag{9}$$

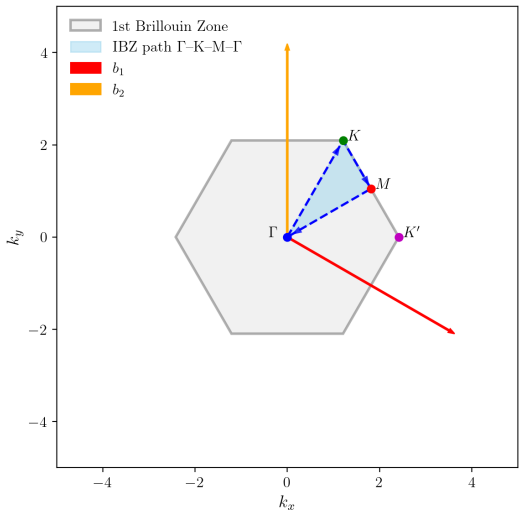

Figure 3: Brillouin zone of the honeycomb lattice and reciprocal lattice vectors $\{b_1, b_2\}$. High symmetry points Γ, K, M, K' labeled, along with the path connecting high-symmetry points over the irreducible wedge of the Brillouin zone.

where the vectors $\{\mathbf{k_1}, \mathbf{k_2}\}$ are chosen to satisfy the relation:

$$\mathbf{k_i} \cdot \mathbf{a_j} = 2\pi\delta_{ij}. \tag{10}$$

We restrict our attention to the two-dimensional time-independent Schrödinger equation for a particle in a periodic potential:

$$-\frac{\hbar^2}{2m}\Delta\psi(\mathbf{x}) + V(\mathbf{x})\psi(\mathbf{x}) = E\psi(\mathbf{x}), \quad V(\mathbf{x} + \mathbf{a_i}) = V(\mathbf{x}). \tag{11}$$

$V(\mathbf{x})$ is, in general, an arbitrary scalar potential, but we enforce that it has the same periodicity as the idealized real space lattice. For suitable choice of units, we can write $m = \hbar = 1$ without loss of generality. Note that equation 11 defines an eigenproblem for complex-valued state wavefunctions $\psi(\mathbf{x})$ and their associated energies (eigenvalues) E, which are guaranteed real by the hermiticity of the Hamiltonian $\mathcal{H}$ in the equivalent statement below:

$$\mathcal{H}\psi(\mathbf{x}) = E\psi(\mathbf{x}), \quad \mathcal{H} \equiv [-\frac{1}{2}\Delta + V(\mathbf{x})]. \tag{12}$$

Due to the periodicity of the system's potential, Bloch's theorem (Ashcroft & Mermin, 2011) allows us to decompose any solution ψ to this problem as the product of a plane wave and a Λ-periodic function, or the *Bloch function* $u_{n,\mathbf{k}}$, as shown below:

$$\psi_{n,k}(\mathbf{x}) = e^{i\mathbf{k}\cdot\mathbf{x}}u_{n,\mathbf{k}}(\mathbf{x}). \tag{13}$$

In equation 13, n indexes the spectrum of allowable energies, and $\mathbf{k}$ corresponds to the *quasi-momentum* of the particle, which is unique in the reciprocal space up to translation with $\mathbf{k_i}$. Also, due to the Λ periodicity of the Bloch function, we obtain the following *pseudo-periodic* boundary condition satisfied by ψ:

$$\psi_{n,k}(\mathbf{x} + \mathbf{a_i}) = e^{i\mathbf{k}\cdot\mathbf{a_i}}\psi(\mathbf{x}). \tag{14}$$

Therefore, with these boundary conditions, we are interested in solving the eigenproblem with $\mathbf{x}$ restricted to the real space Λ unit cell and $\mathbf{k}$ restricted to the reciprocal space primitive cell known as the *Brillouin zone*, encompassing all the points in reciprocal space which are closer to the origin than to any point on the reciprocal latice defined by $\{\mathbf{k_i}\}$. Now, substituting equation 13 into equation 12, we obtain a modified Hamiltonian operator which allows us to solve for the Bloch states directly:

$$\mathcal{H}_b u_{n,\mathbf{k}}(\mathbf{x}) = E_{n,\mathbf{k}}u_{n,\mathbf{k}}(\mathbf{x}), \quad \mathcal{H}_b \equiv [-\frac{1}{2}(\nabla + i\mathbf{k})^2 + V(\mathbf{x})], \tag{15}$$

where every value of $\mathbf{k}$ over the Brillouin zone will produce a discrete eigenspectrum indexed by n, and these $E_n(\mathbf{k})$ functions are known as dispersion surfaces or energy bands.

C HONEYCOMB LATTICE POTENTIALS AND DIRAC POINTS

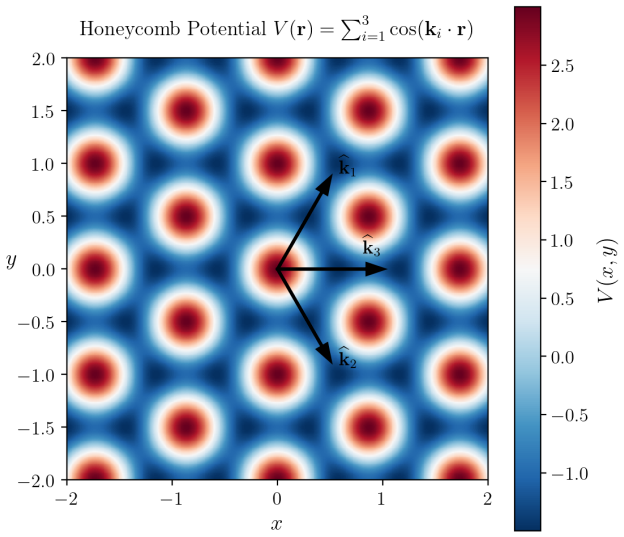

Figure 4: A simple honeycomb lattice potential formed by the superposition of three cosine waves, $V(\mathbf{x}) = V_0 \sum_{i=1}^{3} \cos(\mathbf{b_i} \cdot \mathbf{x})$, where $\mathbf{b_i}$ are the reciprocal lattice vectors.

We begin by considering a triangular lattice Λ_h spanned by vectors, with arbitrary lattice spacing a:

$$\mathbf{a_1} = a \begin{pmatrix} \frac{\sqrt{3}}{2} \\ \frac{1}{2} \end{pmatrix}, \quad \mathbf{a_2} = a \begin{pmatrix} \frac{\sqrt{3}}{2} \\ -\frac{1}{2} \end{pmatrix}, \quad a > 0, \tag{16}$$

and its corresponding dual lattice Λ_h^*:

$$\mathbf{b_1} = q \begin{pmatrix} \frac{1}{2} \\ \frac{\sqrt{3}}{2} \end{pmatrix}, \quad \mathbf{b_2} = q \begin{pmatrix} \frac{1}{2} \\ -\frac{\sqrt{3}}{2} \end{pmatrix}, \quad q \equiv \frac{4\pi}{a\sqrt{3}}. \tag{17}$$

We now define a *honeycomb lattice potential* (Fefferman & Weinstein, 2012; Lee-Thorp et al., 2018), as any real-valued potential $V_h : \mathbb{R}^2 \to \mathbb{R}$ satisfying the following conditions:

1. V_h is periodic with respect to Λ_h, i.e. $V_h(\mathbf{x} + \mathbf{a}) = V_h(\mathbf{x}) \forall x \in \mathbb{R}^2$ and $\mathbf{a} \in \Lambda_h$.
2. V_h is symmetric with respect to inversion, i.e. $V_h(-\mathbf{x}) = V_h(\mathbf{x})$.
3. V_h is invariant with respect to the rotation matrix $\mathcal{R}$ where $\mathcal{R}$ denotes the counterclockwise rotation in $\mathbb{R}^2$ by $\frac{2\pi}{3}$.

For this family of potentials, it can been shown that the above symmetries imply the existence of conical singularities, or *Dirac points*, in the Floquet-Bloch dispersion surfaces at the high-symmetry points K and K' lying at the vertices of the Brillouin zone (Fefferman & Weinstein, 2012; Lee-Thorp et al., 2018). In other words, the dispersion surfaces of the honeycomb lattice exhibit linear band crossings at these high-symmetry points, and the corresponding eigenvalues form a two-fold degenerate spectral pair. The existence of these points give rise to effective massless Dirac fermions in materials such as graphene (Castro Neto et al., 2009), which can be modeled as such a 2D atomic lattice with carbon atoms located at the honeycomb lattice positions.

D NUMERICAL SOLUTION BY PLANE-WAVE EXPANSION

As a ground-truth benchmark, we can employ a convergent numerical solution based on the plane-wave expansion, which yields accurate approximation of eigenvalues and Bloch functions and can be compared to the solutions outputted by the network (Kittel, 2004; Ashcroft & Mermin, 2011).

This approach relies on the Fourier series representation of both the periodic potential and the Bloch functions. For a Λ-periodic potential $V(\mathbf{x})$, we can write:

$$V(\mathbf{x}) = \sum_{\mathbf{K}\in\Lambda^*} V_{\mathbf{K}} e^{i\mathbf{K}\cdot\mathbf{x}}, \quad V_{\mathbf{K}} = \frac{1}{|\Omega|}\int_{\Omega} V(\mathbf{x}) e^{-i\mathbf{K}\cdot\mathbf{x}} d\mathbf{x}, \tag{18}$$

where Ω is the unit cell of the lattice Λ. Similarly, we can express the Bloch function $u_{n,\mathbf{k}}(\mathbf{x})$ as:

$$u_{n,\mathbf{k}}(\mathbf{x}) = \sum_{\mathbf{K}\in\Lambda^*} c_{n,\mathbf{k}}(\mathbf{K}) e^{i\mathbf{K}\cdot\mathbf{x}}. \tag{19}$$

Substituting these expansions into the modified Hamiltonian eigenproblem in equation 15 and projecting onto the plane-wave basis leads to a matrix eigenvalue problem for the coefficients $c_{n,\mathbf{k}}(\mathbf{K})$. By truncating the infinite series to a finite number of reciprocal lattice vectors, we can numerically solve for the eigenvalues and eigenfunctions with controllable accuracy. To see this, we substitute the expansions into equation 15:

$$\mathcal{H}_b u_{n,\mathbf{k}}(\mathbf{x}) = \left[-\frac{1}{2}(\nabla + i\mathbf{k})^2 + \sum_{\mathbf{K}'\in\Lambda^*} V_{\mathbf{K}'} e^{i\mathbf{K}'\cdot\mathbf{x}}\right] \sum_{\mathbf{K}\in\Lambda^*} c_{n,\mathbf{k}}(\mathbf{K}) e^{i\mathbf{K}\cdot\mathbf{x}}. \tag{20}$$

Applying the operator and collecting terms, we have:

$$\begin{aligned} \mathcal{H}_b u_{n,\mathbf{k}}(\mathbf{x}) &= \sum_{\mathbf{K}\in\Lambda^*} c_{n,\mathbf{k}}(\mathbf{K}) \left[\frac{1}{2}|\mathbf{k}+\mathbf{K}|^2 e^{i\mathbf{K}\cdot\mathbf{x}}\right] + \sum_{\mathbf{K}'\in\Lambda^*} V_{\mathbf{K}'} e^{i\mathbf{K}'\cdot\mathbf{x}} \sum_{\mathbf{K}\in\Lambda^*} c_{n,\mathbf{k}}(\mathbf{K}) e^{i\mathbf{K}\cdot\mathbf{x}} \\ &= \sum_{\mathbf{K}\in\Lambda^*} c_{n,\mathbf{k}}(\mathbf{K}) \left[\frac{1}{2}|\mathbf{k}+\mathbf{K}|^2 e^{i\mathbf{K}\cdot\mathbf{x}}\right] + \sum_{\mathbf{K},\mathbf{K}'\in\Lambda^*} V_{\mathbf{K}'} c_{n,\mathbf{k}}(\mathbf{K}) e^{i(\mathbf{K}+\mathbf{K}')\cdot\mathbf{x}}. \end{aligned} \tag{21}$$

Projecting onto the basis function $e^{i\mathbf{Q}\cdot\mathbf{x}}$ for some $\mathbf{Q} \in \Lambda^*$ and integrating over the unit cell Ω, we obtain:

$$\begin{aligned} \int_{\Omega} e^{-i\mathbf{Q}\cdot\mathbf{x}} \mathcal{H}_b u_{n,\mathbf{k}}(\mathbf{x}) d\mathbf{x} = &\sum_{\mathbf{K}\in\Lambda^*} c_{n,\mathbf{k}}(\mathbf{K}) \left[\frac{1}{2}|\mathbf{k}+\mathbf{K}|^2 \int_{\Omega} e^{i(\mathbf{K}-\mathbf{Q})\cdot\mathbf{x}} d\mathbf{x}\right] \\ &+ \sum_{\mathbf{K},\mathbf{K}'\in\Lambda^*} V_{\mathbf{K}'} c_{n,\mathbf{k}}(\mathbf{K}) \int_{\Omega} e^{i(\mathbf{K}+\mathbf{K}'-\mathbf{Q})\cdot\mathbf{x}} d\mathbf{x}. \end{aligned} \tag{22}$$

Using the orthogonality of the plane-wave basis, we find that the integrals evaluate to $|\Omega|$ when the exponents vanish and zero otherwise. This leads to the following matrix equation for the coefficients:

$$\frac{1}{2}|\mathbf{k}+\mathbf{Q}|^2 c_{n,\mathbf{k}}(\mathbf{Q}) + \sum_{\mathbf{K}'\in\Lambda^*} V_{\mathbf{K}'} c_{n,\mathbf{k}}(\mathbf{Q}-\mathbf{K}') = E_{n,\mathbf{k}} c_{n,\mathbf{k}}(\mathbf{Q}). \tag{23}$$

By truncating the set of reciprocal lattice vectors $\mathbf{K}$ to a finite subset, we can numerically solve this matrix eigenvalue problem to obtain approximations of the eigenvalues $E_{n,\mathbf{k}}$ and the coefficients $c_{n,\mathbf{k}}(\mathbf{K})$, from which we can reconstruct the Bloch functions.

E SAMPLING STRATEGY IN REAL AND RECIPROCAL SPACE

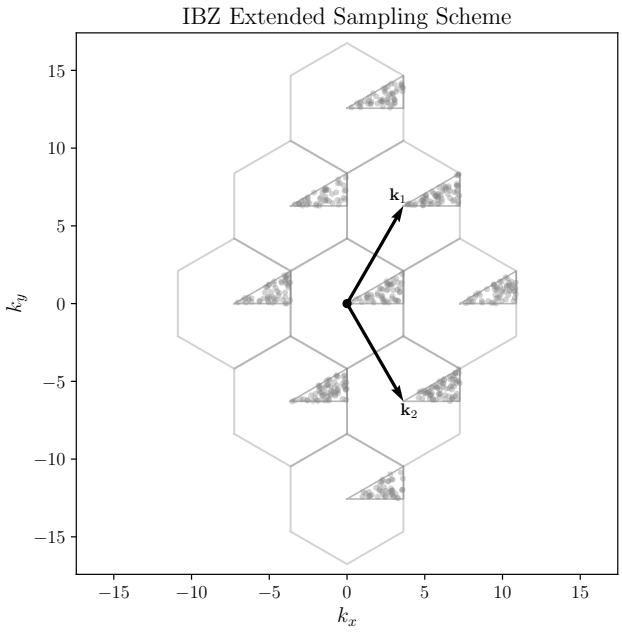

Figure 5: Sampling strategy in reciprocal space. Points are sampled uniformly within the Irreducible Brillouin Zone (IBZ) and its lattice translated copies to expose the network to higher quasi-momenta and energy bands.

In order to effectively train the neural networks, we employ a sampling strategy that covers both the spatial domain of the unit cell Ω and the quasi-momentum space of the Brillouin zone. For the spatial domain, we use uniform random sampling of collocation points within the unit cell spanned by the lattice vectors $\{\mathbf{a_1}, \mathbf{a_2}\}$. This ensures that the network learns to satisfy the Schrödinger equation and boundary conditions throughout the entire unit cell.

As for the quasi-momentum space, we focus on sampling points inside the Irreducible Brillouin Zone (IBZ), which is the smallest wedge of the Brillouin zone that, through symmetry operations, can generate the entire zone. This reduces the computational burden while still allowing the network to learn the essential features of the band structure. We sample $\mathbf{k}$-points uniformly within the IBZ and also from its lattice translated copies to expose the network to higher energy bands.

F ADDITIONAL TRAINING DETAIL

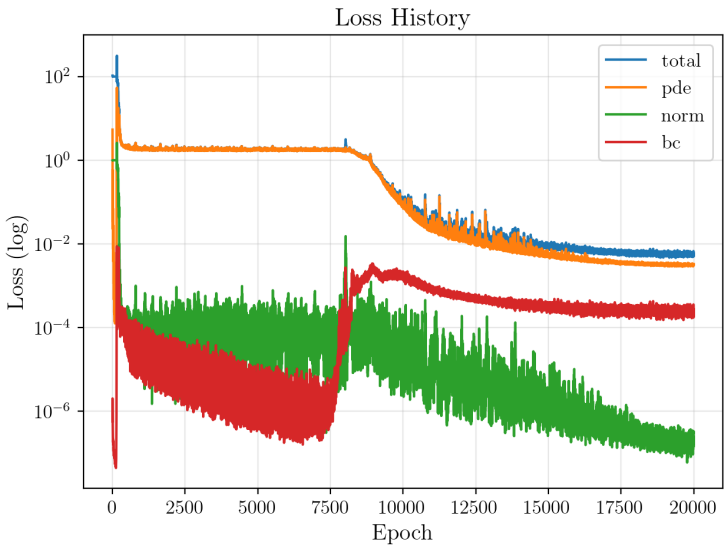

Figure 6: Training loss curves for the physics-informed neural network on the weak honeycomb potential. The total loss and individual components are plotted over training epochs, demonstrating convergence behavior. Around epoch 7500, the network begins to converge to a stable solution and prioritizes minimizing the PDE residual temporarily before settling into a balanced minimization of all loss components.

We train the networks using the Adam optimizer (Kingma & Ba, 2017) with an initial learning rate of $1e-3$, which is combined with a cosine annealing schedule to gradually reduce the learning rate over the course of training. The models are trained for a total of 20,000 epochs with a batch size of 3,000 collocation points sampled per epoch. At each epoch, we compute the total loss $\mathcal{L}$ and backpropagate the gradients to update the network parameters θ and ϕ. To monitor convergence, we track the individual loss components as well as the overall loss throughout training. All experiments were conducted on a single NVIDIA RTX A6000 GPU with 48GB of memory.